

See discussions, stats, and author profiles for this publication at: <https://www.researchgate.net/publication/283717260>

Dynamic DNA Nanotubes: Reversible Switching Between Single and Double-Stranded Forms, and Effect of Base Deletions

ARTICLE *in* ACS NANO · NOVEMBER 2015

Impact Factor: 12.88 · DOI: 10.1021/acsnano.5b04387

READS

65

4 AUTHORS, INCLUDING:



[Janane Rahbani](#)

McGill University

7 PUBLICATIONS 17 CITATIONS

[SEE PROFILE](#)



[Amani A Hariri](#)

McGill University

7 PUBLICATIONS 26 CITATIONS

[SEE PROFILE](#)



[Hanadi F Sleiman](#)

McGill University

112 PUBLICATIONS 3,137 CITATIONS

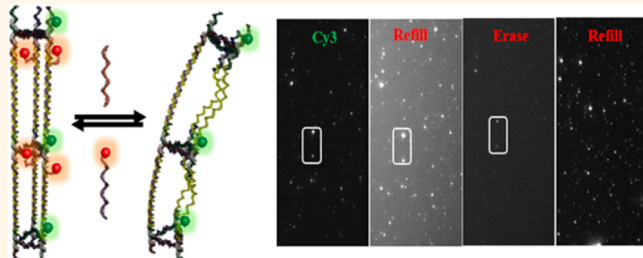
[SEE PROFILE](#)

Dynamic DNA Nanotubes: Reversible Switching between Single and Double-Stranded Forms, and Effect of Base Deletions

Janane F. Rahbani, Amani A. Hariri, Gonzalo Cosa,* and Hanadi F. Sleiman*

Department of Chemistry and Centre for Self-Assembled Chemical Structures, McGill University, 801 Sherbrooke Street West, Montreal, H3A 0B8, Canada

ABSTRACT DNA nanotubes hold great potential as drug delivery vehicles and as programmable templates for the organization of materials and biomolecules. Existing methods for their construction produce assemblies that are entirely double-stranded and rigid, and thus have limited intrinsic dynamic character, or they rely on chemically modified and ligated DNA structures. Here, we report a simple and efficient synthesis of DNA nanotubes from 11 short unmodified strands, and the study of their dynamic behavior by atomic force microscopy and *in situ* single molecule fluorescence microscopy. This method allows the programmable introduction of DNA structural changes within the repeat units of the tubes. We generate and study fully double-stranded nanotubes, and convert them to nanotubes with one, two and three single-stranded sides, using strand displacement strategies. The nanotubes can be reversibly switched between these forms without compromising their stability and micron-scale lengths. We then site-specifically introduce DNA strands that shorten two sides of the nanotubes, while keeping the length of the third side. The nanotubes undergo bending with increased length mismatch between their sides, until the distortion is significant enough to shorten them, as measured by AFM and single-molecule fluorescence photobleaching experiments. The method presented here produces dynamic and robust nanotubes that can potentially behave as actuators, and allows their site-specific addressability while using a minimal number of component strands.



KEYWORDS: DNA nanotechnology · nanotubes · dynamic behavior · stimuli responsive · single-molecule fluorescence

DNA nanotechnology has emerged as a transformational tool for the bottom-up construction of materials. From biophysical probes¹ and electronic devices^{2,3} to drug delivery,⁴ catalysis,⁵ and light harvesting,^{6,7} this approach will impact numerous areas of materials science and medicine.^{8,9} However, progress toward most practical applications, especially *in vivo* work will require more DNA-economic fabrication methods. The challenge here is to balance design simplicity with complex function, so that DNA structures do not need to be made from hundreds of different components, but can still preserve addressability and geometric control. A particularly important property that needs to be maintained in DNA nanostructures is intrinsic dynamic character, allowing them to respond to different stimuli in a predictable manner.

The need to simplify assembly while maintaining programmability and dynamic character is well-exemplified by the construction of DNA nanotubes. The first methods involved the assembly of DNA tile motifs into two-dimensional surfaces, followed by their rolling into nanotubes.^{10,11} This allowed the use of a single DNA strand to assemble an entire nanotube, as an ultimate example of design simplicity.^{12,13} While versatile, this method did not precisely control the tube circumference. A second approach involved the assembly of DNA helix bundles with interconnected parallel DNA helices, thus controlling the tube diameter and geometry.^{14,15} Single-stranded tiles were used to provide double-stranded nanotubes with controlled circumference.^{16,17} The control of nanotube length, diameter and addressability was achieved using DNA origami, from a long genomic scaffold strand

* Address correspondence to hanadi.sleiman@mcgill.ca, gonzalo.cosa@mcgill.ca.

Received for review July 15, 2015 and accepted November 11, 2015.

Published online
10.1021/acsnano.5b04387

© XXXX American Chemical Society

and a large number (hundreds) of different staple strands.^{18,19} Recently, DNA origami tubes were used as “seeds” to control both the onset and circumference of tile-based nanotube assembly.²⁰

These methods result in assemblies that are entirely double-stranded and rigid, and thus have limited intrinsic dynamic character. Our group constructed nanotubes of tunable rigidity and porosity, by organizing triangular or square DNA polygons on top of one another using linking strands.²¹ The resulting tubes can be built in single- or double stranded forms, and the nanotubes can encapsulate cargo and release it by strand displacement.²² This approach required the synthesis of DNA polygons with rigid organic molecules at their corners by cyclization and chemical ligation. The rolling circle amplification (RCA) process was then used to coarsely tune nanotube length and enhance stability, but this method involves cyclization, ligation and enzymatic replication, and it yields double-stranded nanotubes.²³ Recently, we reported two methods to control the length, circumference and patterns on every position of DNA nanotubes, using a temporal growth strategy to sequentially add building blocks.^{24,25} Thus, when nanotubes need to be fully controlled in length and at every one of their positions, the use of DNA origami or sequential construction methods is necessary.

In addition to encapsulation and release, the ability of nanotubes to be dynamic allows their potential use as probes of DNA deformation. DNA can undergo bending, looping and twisting when it interacts with proteins, small molecules, or ions.^{26–29} Because of its fundamental significance, DNA distortion has been the subject of extensive investigation.^{30,31} DNA nanotubes are stiff, extended polymers with repeating segments. As a result, they are potentially capable of binding distorted DNA and amplifying the distortion into a macroscopic change in morphology.³² However, to our knowledge, this morphological switching has not been previously studied. A DNA nanoactuator was incorporated into a 2D-tile lattice by the group of Yan,³³ and DNA structural dynamics have been probed using high speed atomic force microscopy on origami substrates by Sugiyama *et al.*³⁴

We here report a simplified, modular synthesis of DNA nanotubes, and the investigation of their structural switching by strand displacement strategies, using atomic force microscopy and *in situ* single molecule fluorescence microscopy. These nanotubes have controlled geometry and circumference, and can be site-specifically and reversibly switched between single and double-stranded forms. The method relies on only 11 unmodified DNA strands and involves no ligation or RCA steps, thus it can be readily applied by any laboratory. The unique architecture of our nanotube is capable of amplifying DNA distortion into a measurable morphological change. First, we “peel off”

and “refill” strands in different numbers and locations on an immobilized nanotube, examine the stability of the single-stranded version of the design, and study the morphological switching between the single and double-stranded forms. Second, we increasingly shorten two nanotube sides while keeping the third constant, resulting in length mismatch in each repeat unit. We show the bending of the nanotubes, until the distortion is significant enough to shorten the nanotube, as measured by AFM and by single molecule photo-bleaching studies. The latter method quantifies the number of repeat units within the nanotube.^{35,36} We explore the mechanism that underlies the formation and elongation of the nanotube, and the appearance of shorter tubes with increasing length mismatch.

RESULTS AND DISCUSSION

Our nanotube synthesis starts with a triangular “core” unit (U), composed of 6 unmodified DNA strands (Figure 1A). The mixture is annealed at 95 °C then slowly cooled down to 4 °C over 4 h to give (U) in quantitative yield (Figure 1A, left, polyacrylamide gel electrophoresis (PAGE)). The core structure (U) possesses extensions from the top and bottom of the triangular plane, in order to hybridize *via* sticky-end cohesion to three linking strands (LS1–3), which result in nanotube formation. To maximize the yield of fully formed nanotubes and prevent cross-linking, our method uses linking strands that are different from one another (Figure 1B). The first, LS1 is designed with longer sticky-ends (14 nucleotides, nt), and the other two (LS2, LS3) with shorter sticky-ends (10 nt). The nanotubes T1 are formed through a stepwise, hierarchical mechanism. Linking strand LS1 is first added (heating to 56 °C then cooling to 22 °C), resulting in the formation of an open structure T_{op} with the triangular rungs positioned on top of one another (Figure 1B). Then linking strands LS2 and LS3 are added (44 to 22 °C) to close the structure T_{op} with preorganized triangles, into the full nanotube (see Supporting Information). Finally, the elongation of the tubes occurs when the strands are geometrically well aligned, as demonstrated below. The self-assembly of tubes T1 was initially examined by nondenaturing agarose gel electrophoresis (AGE) and atomic force microscopy (AFM). AGE shows the formation of a non-penetrating band consistent with a large structure, while AFM shows long and stiff tubes ranging between 1 and 3 μ m in length (Figure 2A, mean length: 1403 nm; standard deviation (SD): 796.1 nm).

Single-molecule total internal reflection fluorescence microscopy (TIRFM) was used to obtain quantitative information on the nanotube formation. For this, we created a nanotube T1 where the core triangular unit is singly labeled with a Cy3 dye (Figure 2B; LS2 and LS3 have the same sequence in the middle, double-stranded portions, but different sequences at their sticky-end regions). In order to immobilize the

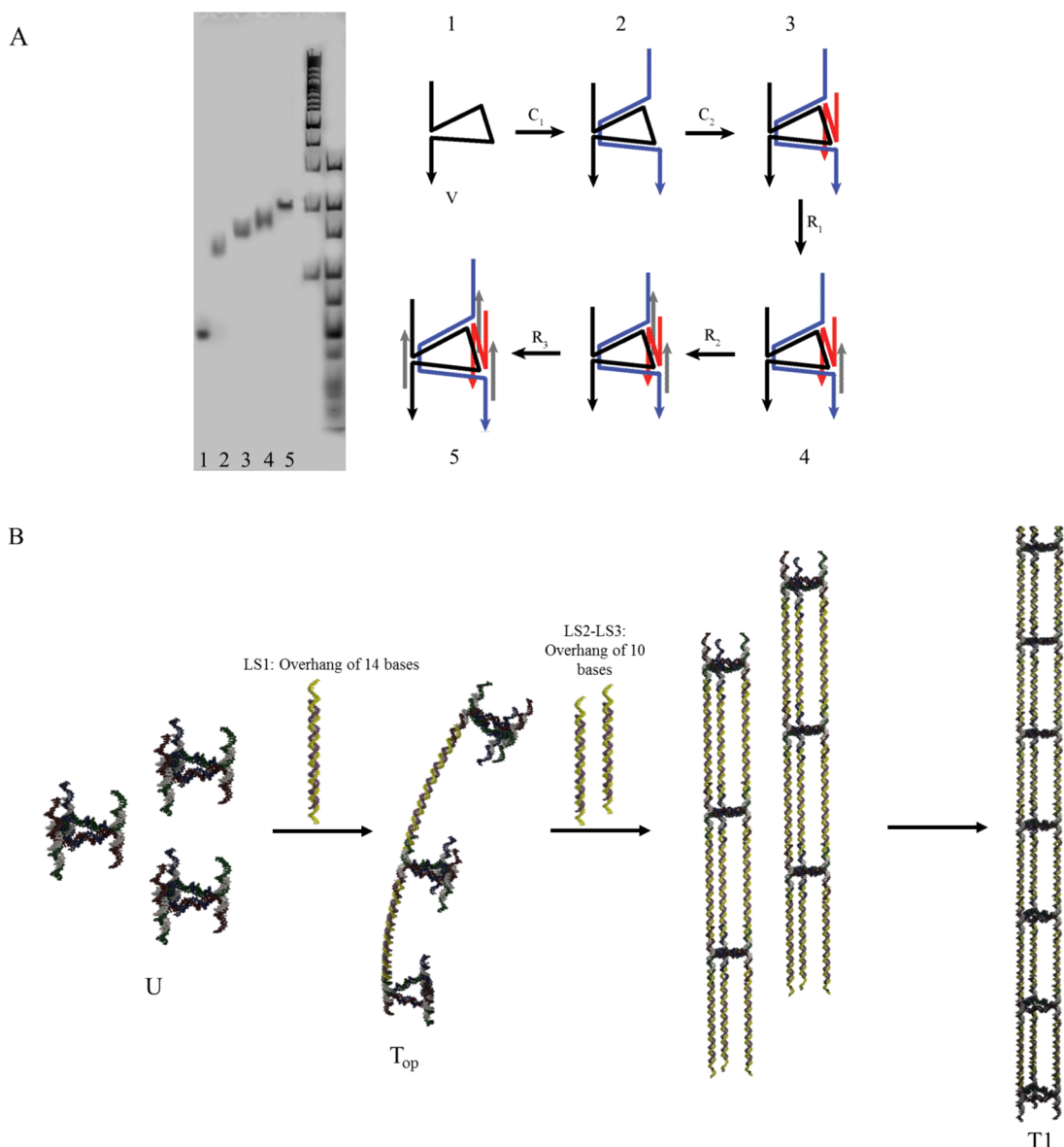


Figure 1. DNA nanotube design. (A) Assembly of the triangular core unit U from 5 unmodified DNA strands. (Right) Design of U: Strand V (black) binds with complementary strand C1 (blue), which spans its internal section and creates a core triangular frame. Complementary strand C2 (red) binds the third edge. Rigidifying strands R1, R2 and R3 (gray) bind the overhangs of C1 and C2, holding them out of plane from the triangular core, to create the vertical sticky-ends of the rung. (Left) 8% non-denaturing Polyacrylamide gel electrophoresis (PAGE) characterization of the stepwise assembly of the triangular core unit U. Lanes 6 and 7 represent the O'Gene Ruler DNA ladder mix (100–10000 base pairs) and the ultralow range DNA marker (10 to 300 base pairs) respectively. (B) Stepwise nanotube formation through sticky-end cohesion of the rung units to LS1 first, to form T_{top} , then of LS2/LS3, followed by tube elongation.

nanotubes on a coverslip surface, 5% of one of the strands within the triangular core were also labeled with biotin (Figure 2B). The 5% average biotin labeling represents a compromise between specifically immobilizing the nanotubes on the coverslip surface and maintaining their dynamic character. Polycarbonate film imaging chambers were assembled onto glass coverslips, coated with a mixture of polyethylene glycol (PEG) and biotin-tagged PEG to prevent non-specific adsorption. Individual dye-labeled nanotubes were next specifically immobilized on the coverslips via biotin–streptavidin interactions.³⁷ We expect most

nanotubes to bind partially in a side-on manner to the PEG-streptavidin surface (Figure 2B). Regions were excited using a TIRF setup with an evanescent field employing the 532 nm output of a diode laser. Images corresponding to a field of view of *ca.* 70 $\mu\text{m} \times$ 35 μm were acquired on an EMCCD camera. Typically 150 single DNA nanotubes were simultaneously imaged within this field of view (Figure 2C).

We used single molecule photobleaching to count the number of Cy3 dyes, and thus the number of repeat units, in each single nanotube imaged. Here, images were acquired for extended periods of time enabling

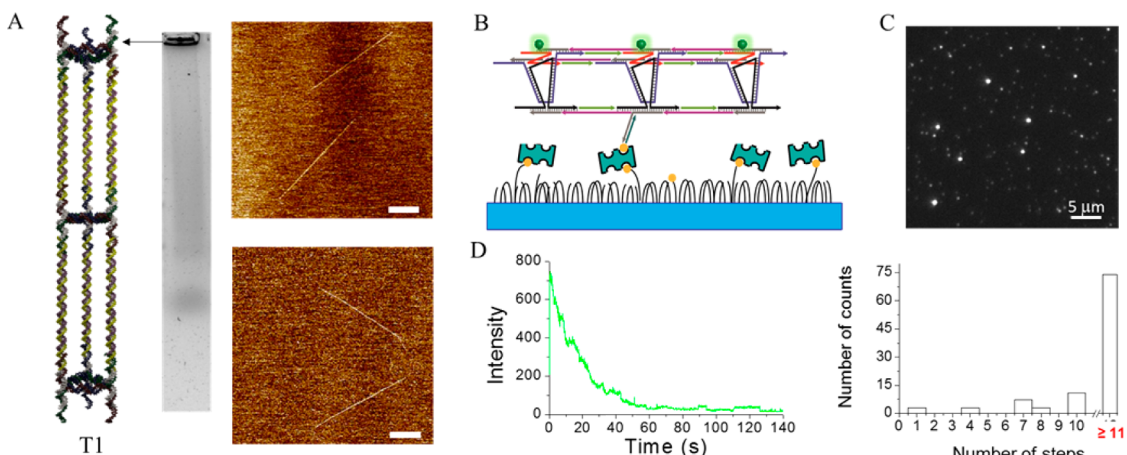


Figure 2. Characterization of the nanotube formation. (A) 1% nondenaturing agarose gel of tubes T1 showing a nonpenetrating band. Two AFM micrographs displaying straight nanotubes with a length ranging from ~1 to 3 μm (scale bar: 500 nm, see Supporting Information for additional images). (B) Schematic illustration showing the immobilized nanotubes on the PEG-streptavidin coated coverslip surface. (C) Typical TIRFM image of surface-bound Cy3 labeled nanotubes, scale bar 5 μm . (D) Typical intensity-time trajectory acquired for a single nanotube with a histogram showing the distribution of the number of steps (Cy3 dyes) obtained from photobleaching curves.

visualizing the intensity time profile of individual nanotubes.^{38,39} Conditions were optimized to work under the full dynamic range of the imaging camera, avoiding saturation by the larger structures. Considering that the structures are ~2 μm long on average by AFM, we expect an average of 70 Cy3 dyes per nanotube. Given the noise in single molecule trajectories, we have observed that up to 10 dyes in a structure may yield discrete photobleaching steps in the intensity-time trajectory, essentially a “staircase” photobleaching pattern. The number of intensity steps may be counted and the number of Cy3 repeats and thus the nanotube length can thus be quantified. Nanotubes with more than ca. 11 dyes exhibit however steps that are too small, and not sufficiently separated over time, to be unambiguously assigned. In this case the intensity time trajectory shows rather an exponentially decreasing intensity over time. In the case of tube T1, we observed photobleaching patterns with an exponentially decreasing intensity for the majority (90%) of the single nanotubes imaged. A histogram reflecting the Cy3 count distribution is displayed in Figure 2D.

We next performed single molecule photobleaching studies to determine whether the elongation of our nanotubes into micron-sized structures occurs in the first step of their formation (upon LS1 binding) or in the second step (upon LS2/3 binding). We assembled the 5%-biotin and Cy3-labeled nanotubes by solution annealing the components with LS1 only, but without LS2 and LS3. This is expected to give a Cy3-labeled open, intermediate structure T_{op} (Figure 1B). Gel electrophoresis shows bands of higher mobility compared to the full nanotube band (Supporting Information Figure S1), consistent with shorter features. Attachment of these open forms onto the coverslip surface

and examination of their length by single-molecule TIRFM with photobleaching revealed a maximum of 10 rungs in the histograms, and the complete absence of structures with exponential intensity decrease traces (Figure 3). These observations are consistent with the formation of relatively short structures in the first step (Figure 1B). We believe that LS2 and LS3 bind these open structures to form short closed tubes that are geometrically well-aligned now to grow and elongate through base pairing of the sticky ends. (Figure 1B). Tile-based nanotubes have been shown to form through a nucleation-elongation mechanism, with a relatively high barrier for the assembly of a few tiles into a short nanotube core, followed by facile elongation of the nuclei.⁴⁰

We next explored the potential to address DNA nanotubes in response to site-specific DNA hybridization events. To date, DNA nanotubes have not been employed as potential nanomechanical devices. A key challenge is to develop an understanding of their collective structural changes in response to modifications in their repeat unit. In the present nanotubes, the linking strands LS1, LS2, and LS3 can be independently addressed (note that LS2 and LS3 have the same sequence in their middle, double-stranded portions, but different sequences at their sticky-end regions). Two strategies were used: (i) switching between single- and double-stranded forms of the nanotube upon displacing one, two and three complementary strands of the linking strands (LS1–3), and (ii) switching to nanotubes where two sides are shorter than the third one, by a specified number of bases. We investigated the morphological changes by AFM and single-molecule fluorescence microscopy, including *in situ* experiments. For the latter experiments, in addition to Cy3 labeling of the core triangular units, we labeled the two linking

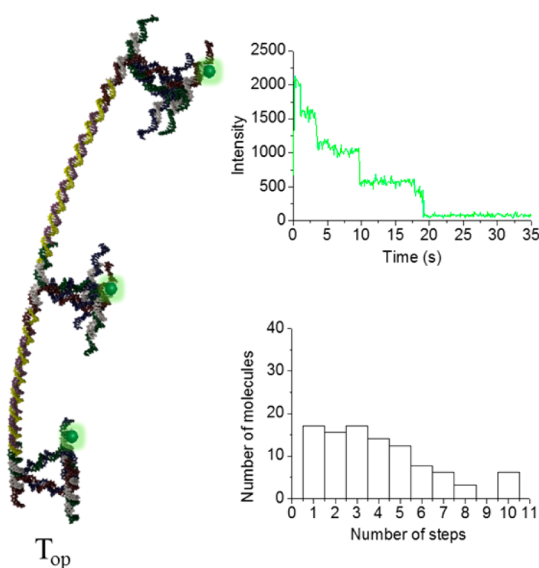


Figure 3. Single molecule characterization of the open tube. Left: Schematic illustration of the Cy3-labeled open tube immobilized on coverslips via biotin–streptavidin interactions, and studied by TIRF. Top right: Typical intensity–time trajectory acquired for a single open nanotube, displaying 5 steps (dyes). Bottom right: Histogram showing the distribution of the number of steps (Cy3 dyes) obtained from photobleaching curves of the open nanotube samples.

strands bearing short sticky ends (LS2 and LS3) with the red emitting dye Atto647N. Using two different diode lasers, regions were excited with an evanescent field first at 641 nm and then at 532 nm. This sequential recording of the frames minimized artifacts that arise from the bleeding of Atto647N emission into the green channel and of Cy3 emission into the red channel. Single frames (200 ms) were acquired to prevent the photobleaching of the dyes. We expect little FRET between the dyes because of their large separation (~ 7 nm, Supporting Information VIII). For the doubly labeled surface-anchored nanotube, we observed the spatial colocalization of the two dyes (Cy3 and Atto647), consistent with retention of nanotube integrity upon immobilization.

We first applied a strand displacement strategy to erase and refill the complementary strands of LS1, LS2 and LS3 in solution.⁴¹ To accomplish this experiment, we built the tubes using extended linking strands LS1–3*, bearing the same sequence as the original LS1–3, but additionally carrying a 10-base overhang. We then added fully complementary strands (eraser strands E1–3) that are expected to bind to each of LS1–3* thus displacing them one by one from the nanotube. This leaves the nanotube single-stranded on one, two and three sides respectively (1ssT, 2ssT and 3ssT in Figure 4A). We examined each state of these tubes *in situ* by TIRFM and observed their conformation by AFM.

The partially single-stranded tubes 1ssT and 2ssT were deposited on a freshly cleaved mica surface.

Interestingly, AFM (in air) shows that making one- or two sides single-stranded does not significantly change the average tube length (Figure 4B and S6A). However, one can immediately notice the shift from straight tubes on the mica surface to curved, especially in 2ssT (where the mean bending angle value is 20° and the standard deviation (SD) is 6.9° , see Figure S6B), when two sides were single-stranded. We have manually counted the number of curved *versus* straight tubes, using the AFM images and we have found that 93% of the 2ssT tubes were curved compared to 80% for 1ssT. The fully single-stranded tubes 3ssT (Figure 4B) revealed curvature (97% curved tubes, mean angle value: 25° ; SD: 9.1°), with a decrease in the population of individual tubes on the surface. At the same concentration, 3ssT tubes tended to form bundles under the dry AFM conditions (possibly due to their increased flexibility). We then added LS1–3* again to the fully single-stranded tubes 3ssT in solution, to examine whether we could reconstitute their double-stranded form. By AFM, the tubes adopted again their original linear conformation. Interestingly, reconstituted tubes have similar length distribution as the original unmodified versions (mean length value: 1400 nm; SD: 800 nm), as depicted in Figure 4B and Figure S6A. By gel electrophoresis, the three nanotube forms (double, partially single, and single-stranded) all showed nonpenetrating bands, indicating the assembly of large structures consistent with the AFM results. (Supporting Information, Figure S2)

To further examine the system dynamics, we carried out *in situ* single molecule TIRF studies. We immobilized the nanotubes T1 labeled with Cy3 and 5% biotin as before, but we used in this case ATTO647N-labeled LS2/3*, containing 10-bases overhangs. We once again observed the spatial colocalization of the two dyes in most of the imaged structures (Figure 5B). We then added the erasing strand E2/3 at a concentration of 500 nM (in excess), to form the immobilized, partially single-stranded nanotube 2ssT. This was followed by a washing step with 1× TAMg buffer (50 μ L). Consistent with two sides of the nanotube losing the labeled LS2/3* and becoming single stranded, no emission was detected on the red channel (Atto647N) following the above 2 steps. We next added and incubated fresh ATTO647N-LS2/3* solution at a concentration of 500 nM (in excess) followed by a washing step with 1× TAMg buffer (50 μ L). Co-localization of the two dyes indicated the success of the refilling experiment. Interestingly, refilling the partially single-stranded tube 2ssT with strands was qualitatively slow, taking tens of minutes, in contrast with the near immediate removal of the strands from double-stranded tube T1. We are currently exploring the reason for the qualitatively different rates of erasing and refilling observed. When we compare the intensity ratios of the two dyes before and after erasing/refilling, we notice a high refilling percentage

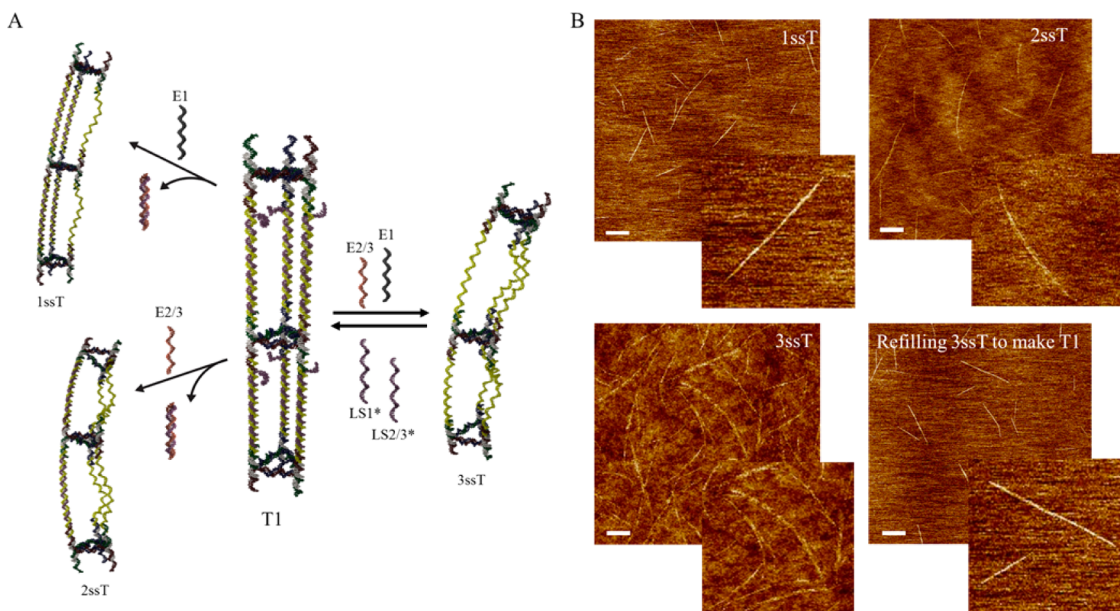


Figure 4. Strand displacement experiment. (A) Schematic showing the addition of the erasing strand E1 to generate tubes with one single-stranded side 1ssT, the addition of E2/3 to produce tubes with two single-stranded sides 2ssT and the hybridization of both E1 and E2/3 to form the fully single-stranded version of the tubes 3ssT. The original tube T1 is reconstituted upon addition of LS1* and LS2/3* to 3ssT. (B) Dry AFM micrographs (scale bar 500 nm) depicting the morphological changes of the tubes upon E1 and/or E2/3 addition (insets are magnified images for single features; see Supporting Information for additional images). The curvature of the constructs increases as they become more single-stranded. The initial linear morphology is recovered after refilling these single-stranded portions. In these images, care was taken to avoid washing the mica surface with water after deposition, in order to preserve the native nanotube structure (see SI). As such, some salts remain on the surface in the AFM images.

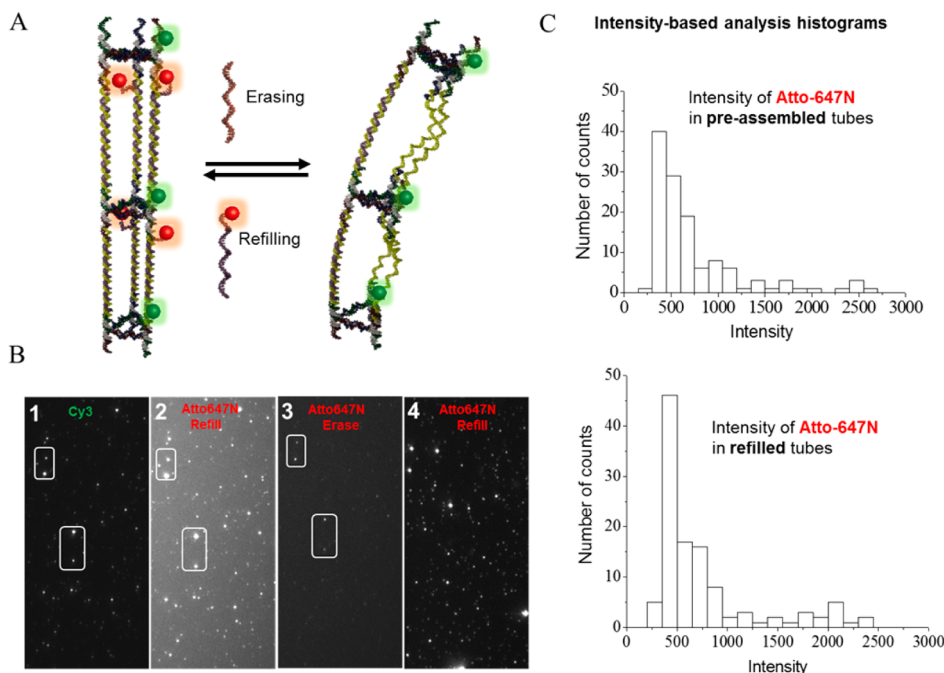


Figure 5. Single-molecule characterization of the reversible switching between tubes T1 and 2ssT, immobilized on coverslips using biotin–streptavidin interactions. (A) Schematic showing the removal of the strands labeled with Atto647N and their readdition. (B) Series of TIRFM images ($70 \mu\text{m} \times 35 \mu\text{m}$) displaying the colocalization of the two dyes prior to the removal of the labeled LS2/3* (panels 1 and 2), the disappearance of the Atto647N emission upon adding E2/3 (panel 3) and its reappearance after LS2/3* hybridization (panel 4). (C) Histograms depicting the intensity distribution of Atto647N in preassembled versus refilled tubes T1, consistent with efficient refilling with LS2/3*.

after 1 h incubation. These observations provide evidence of the stability of the tubes in both single- and

double-stranded forms and their ability to restore the initial design without degradation (Figure 5C). We note

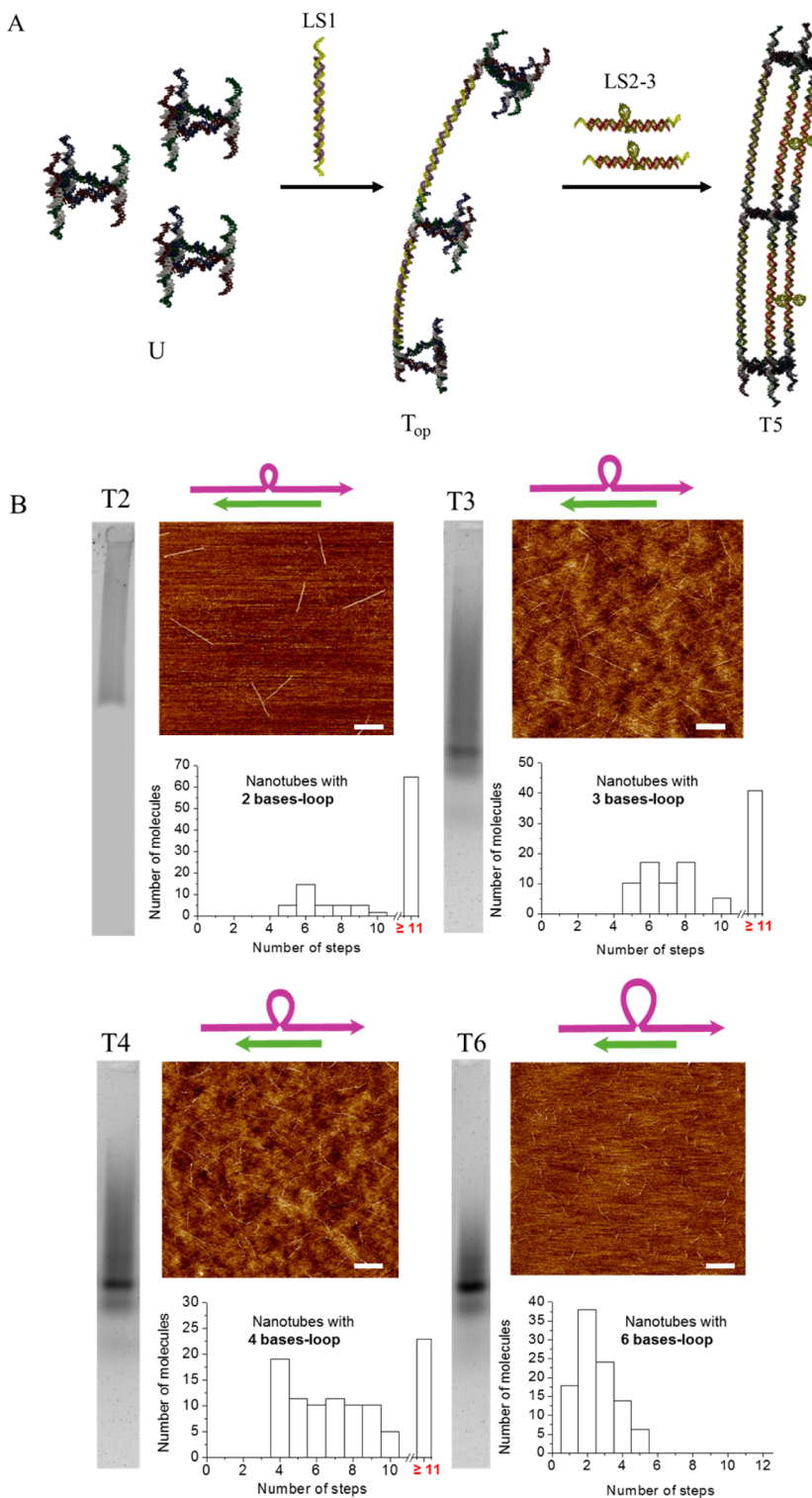


Figure 6. Study of the robustness and morphological changes of the tubes by increasing length mismatches between the vertical strands of the repeat units. (A) Schematic representing the introduction of a size mismatch between LS2–3 strands and LS2/3* through a gradual decrease of the length of LS2/3* strand. (B) Characterization of the effect of these mismatches on the shape and size distribution of the tubes by 1% nondenaturing AGE, AFM (scale bar 500 nm) and TIRFM. The average length of the tubes decreases with increasing the mismatch length; a mismatch of 5 bases is enough to break the tubes into small pieces of 5 rungs at most. For the AGE of T2, the band of very low mobility is faint; we speculate that the length mismatch in T2 slightly weakens its sticky-end interactions, such that the tube fragments as it travels down the AGE gel.

the difference in the background between panel 2 and panel 3, and between panel 2 and panel 4 in Figure 5B.

This difference is due to the incubation of the Atto647N labeled DNA in the chamber (panel 2) giving higher

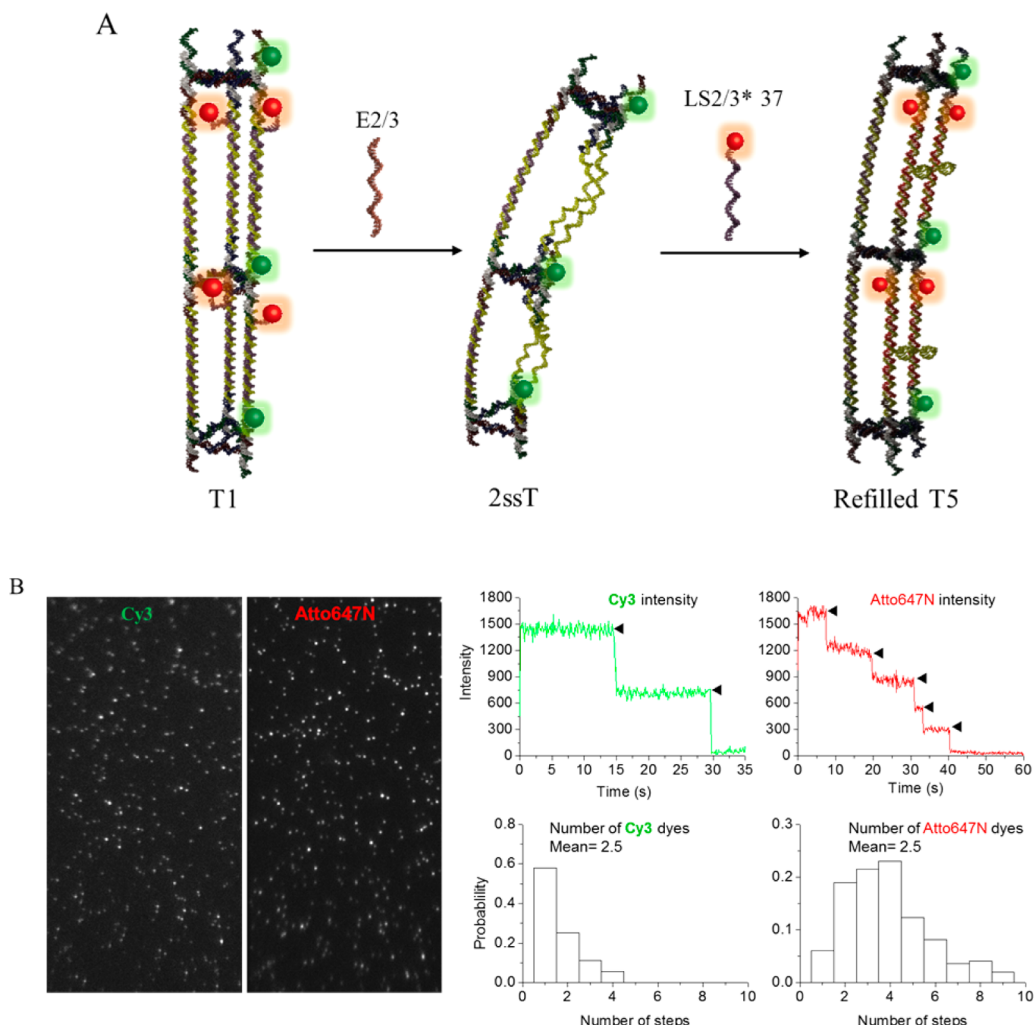


Figure 7. Single-molecule characterization of tubes T1 treated in solution with E2/3, then refilled with 5-base length-mismatched LS2/3*, resulting in T5. This is followed by immobilization on the coverslip surface and TIRF measurement. (A) Schematic of the experiment. (B) TIRF images displaying the colocalization of the two dyes Cy3 and Atto647N ($70 \mu\text{m} \times 35 \mu\text{m}$). Photobleaching traces and histograms of the probability distribution of the number of steps in the traces of refilled T5 showing that the majority of the tubes consist of two to three rung units.

background, which is rinsed thoroughly (panel 3) after erasing. Panel 4 is also a refill with Atto647N labeled DNA but in this case after rinsing thoroughly, not during incubation as in panel 2.

These experiments are consistent with the ability to reversibly cycle the nanotube system between double-stranded, partially single-stranded and fully single-stranded forms. The nanotubes are increasingly curved as they become more single-stranded in character (AFM). Our preliminary evidence shows that the surface attached single-stranded nanotubes are slower to rehybridize into their double-stranded form (TIRF), possibly consistent with increased DNA deformation and/or compaction and decreased accessibility. The switching processes are reversible, and the nanotube retains its length and robustness as it changes between these forms.

In the next set of experiments, we modified the length of the strand complementary to the two linking

strands (LS2/3* as shown in Figure 6A) by removing 2 to 6 bases. By hybridizing to LS2/3*, these shorter strands likely cause the formation of internal loops of 2 to 6 bases. As a result, on one side of the nanotube, two consecutive triangular cores are separated by 84 bases ($\sim 28.6 \text{ nm}$) and on the other two sides they are separated by shorter DNA stretches: 82 for T2 ($\sim 27.9 \text{ nm}$), 81 for T3 ($\sim 27.5 \text{ nm}$), 80 for T4 ($\sim 27.2 \text{ nm}$), 79 for T5 ($\sim 26.9 \text{ nm}$) and 78 bases for T6 ($\sim 26.5 \text{ nm}$) respectively. This size mismatch repeats over the whole length of the nanotube at each constitutive polygon (a $1 \mu\text{m}$ nanotube has ~ 35 repeat LS units).

Strategies for bending DNA nanostructures have been developed by the Shih, Yin and Yan groups, by introducing insertions and deletions, or placing designed crossover and nick points at specific positions.^{42–44} Here, rather than introducing static structural changes, we examine the dynamic switching

of nanotubes between different states. The length mismatch between the tube sides serves as a model for a local DNA structural change in the repeat unit (distortion/bending as a result of protein or small molecule binding). We were interested to probe whether this mismatch results in morphological changes in the nanotubes, and at which point this bending/distortion would disrupt nanotube formation.

We used two methods for the generation of these modified nanotubes. First, the nanotubes were pre-assembled in solution by mixing and annealing all strands. They were studied by nondenaturing AGE, AFM under dry conditions and TIRFM. As described earlier (Figure 2), fully double-stranded T1 shows a nonpenetrating band by AGE, straight and long features by AFM (~ 70 rungs) and exponential traces in intensity trajectories. As the length difference between the tube sides increases (T2–T6), AGE shows smeared bands of progressively higher gel mobility, consistent with shorter nanotubes (Figure 6B). By AFM, tubes T2 with a difference of 2 bases were not able to grow more than $\sim 1 \mu\text{m}$ (~ 35 rungs, Figure 6B). The mean length was calculated to be 720 nm (SD: 375.3 nm) and 80% of these tubes were curved (Figure S7A). 94% of tubes T3 showed a certain degree of curvature with a mean bending value of 19° (SD: 8.4°) (Figure S7B), and structures with a mean length value of 590 nm (SD: 186.6 nm) were imaged. Single molecule TIRFM photobleaching experiments for T2 and T3 showed an exponential decay for the majority of the tubes, with a slight increase in the population of shorter tubes made up of 5 to 10 repeat units (Supporting Information, Figure S10). With a 4 bases difference between LS1 and LS2/3, 96% of the tubes appeared to be curved (mean: 21° ; SD: 9.7°) but with a length of ~ 500 nm (~ 18 rungs) at most (mean length: 226 nm; SD: 96.2 nm). By TIRFM, T4 exhibits a large increase in the population of shorter tubes ranging from 4 to 10 rungs, with only $\sim 33\%$ of the tubes showing an exponential decay (Figure S10).

A difference between the three sides of the tubes of 5 and 6 bases induced the assembly of small features of ~ 150 nm and less (~ 5 rungs, Figure 6B). Using single molecule photobleaching, we generate histograms of the distribution of the number of steps in the nanotubes, where tubes T5 and T6 showed short nanotubes with no more than 5 repeat units (Figure 6B). Thus, the introduction of length mismatch in the repeat units of DNA nanotubes results in bending for differences of 2–3 bases, with relative maintenance of the tube length. On the other hand, a mismatch greater than 4 bases introduces sufficient distortion to cause nanotube shortening, which becomes significant for differences of 5–6 bases. We have carried out control experiments on a DNA dimer model of the nanotube, to verify proper hybridization of the length mismatched form (Figure S4).

Length mismatched nanotubes can also be generated directly from the partially single stranded form 2ssT. In particular, we were interested to see if an initially long single-stranded nanotube 2ssT can be fragmented and shortened upon addition of length mismatched strands, even under mild conditions. In solution, we generated 2ssT with Cy3 and 5% biotin, by starting with double-stranded T1 and strand displacement of LS2/3 (Figure 7A). We then refilled the tube with the 5-bases shorter complements (LS2/3* 37) labeled with Atto647N, in solution at room temperature (1 h incubation). Immobilization of these preformed nanotubes T5 followed by TIRF showed the colocalization of Cy3 and Atto647N in the expected 1:2 ratio, consistent with a high refilling yield. Cy3 photobleaching revealed the presence of short nanotubes, with no more than 5 repeat units (Figure 7B). Short structures similar to tubes T5 were also observed by AFM after the addition of LS2.3* (5-base shorter) in solution (Figure S3). Thus, preannealing nanotubes T5 with length mismatch, or generating them from single-stranded forms produce similar populations of shortened nanotubes. We are currently investigating whether the nanotube length can be correlated with the extent of distortion introduced in the DNA strands within the repeat unit: this would allow the nanotube to act as a reporter of small molecule- or protein-induced DNA binding events.

CONCLUSIONS

In conclusion, we have shown a simple and efficient synthesis of DNA nanotubes from 11 short unmodified strands. This yields robust structures with controlled geometry and circumference, and site-specific addressability. Unlike tile- or origami-based structures, these nanotubes can be reversibly switched between a fully double-stranded form, and structures with one, two or three single-stranded repeat units. We show by atomic force microscopy that this results in bent and flexible structures. *In situ* fluorescence microscopy shows that strand displacement from double-stranded forms occurs quickly, but the “refilling” of single-stranded forms occurs more slowly, consistent with their increased flexibility and possible compactness. Interestingly, refilling the single-stranded structures to go back to the double-stranded tube is very efficient, pointing to the robustness of this nanotube “actuator”. We introduce an additional morphological change into the nanotubes: an increasing size mismatch between the vertical strands of each repeat unit. This results in nanotube bending, until the introduced distortion disrupts the formation of long nanotubes. Because they have a large number of repeat units down their length, these nanotubes have the potential to amplify biologically relevant DNA distortions. Thus, this method allows the simple and scalable

production of dynamic nanotubes, for potential applications as biophysical probes, tools for drug

delivery, materials organization, plasmonic scaffolds and nanowire growth.

MATERIALS AND METHODS

Materials. Acetic acid, boric acid, EDTA, urea, magnesium chloride, GelRed, tris(hydroxymethyl) aminomethane (Tris), D(+)-glucose, 2-betamercaptoethanol, and streptavidin were purchased from Aldrich. Nucleoside (1000 Å)-derivatized LCAACPG solid support with loading densities of 25–40 μmol/g, Sephadex G-25 (super fine DNA grade), and reagents for automated DNA synthesis were used as purchased from BioAutomation. Acrylamide (40%)/bis-acrylamide 19:1 solution and agarose were purchased from BioShop. For TIRFM sample preparation, 1% v/v Vectabond/acetone was purchased from Vector Laboratories, while poly(ethylene glycol) succinimidyl valerate MW 5000 (mPEG-SVA) and biotin-PEG-SVA were purchased from Laysan Bio, Inc. Imaging chamber components were purchased from Grace Bio-Lab. AFM cantilevers were purchased from Asylum Research (model AC160TS) and RubyRed mica were ordered from Electron Microscopy Sciences. TBE buffer is composed of 90 mM Tris and boric acid and 1.1 mM EDTA, with a pH of ~8.3. TAMg buffer is composed of 45 mM Tris and 12.5 mM MgCl₂ with a pH of ~7.8 adjusted by glacial acetic acid.

DNA Nanotubes Design. The sequences were generated by the Canada 2.0 software (available online). The strands were synthesized via automated solid-phase synthesis carried on a BioAutomation MerMade MM6 DNA synthesizer. Labeled strands were ordered from Integrated DNA Technologies (IDT). The strands were quantified by UV-vis spectroscopy with a Nano-Drop Lite Spectrophotometer and using IDT's extinction coefficient at 260. Please refer to the Supporting Information for more details on the design and the sequences.

Nanotubes Synthesis. The triangular rung unit was the result of the assembly of 6 unmodified strands (V: 113 bases, C1:84 bases, C2:63 bases and R1, R2 and R3:22 bases) in equimolar mixture with a final concentration of 136 nM in 1× TAMg. The solution was annealed from 95 to 4 °C over 3 h 40 min to get the highest yield possible of the clean product. The formation of the rung was confirmed by native polyacrylamide gel electrophoresis (PAGE: 20 × 20 cm vertical Hoefer 600 electrophoresis unit) shown in the Supporting Information. The optimization of the length of the six sticky ends coming out from each rung unit is further discussed in the paper and in the Supporting Information. In order to form the nanotube, 1 equiv of the first set of linking strands LS1 was added. LS1 hybridized to two sticky-ends during an annealing step from 56 to 22 °C for 1 h. The preorganized opened assembly was closed to the full nanotube after the addition of 1 equiv of each of the two linking strands LS2 and LS3 and their complements while annealing the mixture from 44 to 22 °C for 45 min. The formation of the tubes was first characterized by a 1% nondenaturing agarose gel (Owl Mini gel electrophoresis unit) stained 20 min in GelRed.

AFM Imaging. AFM was carried on with a MultiMode 8 SPM connected to a Nanoscope controller, from the Digital Instruments Veeco Metrology Group. 5 μL of various forms of nanotubes at a concentration of 100 nM in filtered 1× TAMg were deposited on freshly cleaved mica then incubated for at least 1 h under a vacuum. Deposition conditions and supplementary micrographs are given in the Supporting Information.

Fluorescence Spectroscopy. Coverslips were washed, labeled with polyethylene glycol, and functionalized with streptavidin as detailed in the Supporting Information. Nanotubes were deposited via biotin–streptavidin interactions then imaged via a two-color total internal reflection fluorescence microscopy setup. The photobleaching events were recorded and fluorescence intensity time traces of individual molecules were analyzed using a self-written algorithm in IDL and Matlab. A detailed description of imaging conditions is outlined in the Supporting Information.

Conflict of Interest: The authors declare no competing financial interest.

Acknowledgment. G.C and H.F.S thank NSERC, CFI, CSACS, the CIHR Drug Development Training Program, the NSERC CREATE training program in Bionanomachines and FQRNT for funding. H.F.S. also thanks CIFAR and CHRP. H.F.S. is a Cottrell Scholar of the Research Corporation. The authors thank Alexander Rousina-Webb for graphical illustrations in the manuscript figures.

Supporting Information Available: The Supporting Information is available free of charge on the ACS Publications website at DOI: 10.1021/acsnano.5b04387.

Detailed design of the nanotubes, DNA sequences and experimental procedures starting from the synthesis of a single DNA strand until the assembly of the entire series of the nanotubes, AGE experiments on the switching between T1 and 1sst, 2ssT, 3ssT and T5, dimer experiments, additional AFM images showing the morphological changes between the different nanotube forms and TIRFM control imaging and analysis. (PDF)

REFERENCES AND NOTES

- Jain, A.; Liu, R.; Ramani, B.; Arauz, E.; Ishitsuka, Y.; Ragunathan, K.; Park, J.; Chen, J.; Xiang, Y. K.; Ha, T. Probing Cellular Protein Complexes Using Single-Molecule Pull-Down. *Nature* **2011**, *473*, 484–488.
- Park, S. H.; Yan, H.; Reif, J. H.; LaBean, T. H.; Finkelstein, G. Electronic Nanostructures Templated on Self-Assembled DNA Scaffolds. *Nanotechnology* **2004**, *15*, 525.
- Liu, D.; Park, S. H.; Reif, J. H.; LaBean, T. H. DNA Nanotubes Self-Assembled From Triple-Crossover Tiles as Templates for Conductive Nanowires. *Proc. Natl. Acad. Sci. U. S. A.* **2004**, *101*, 717–722.
- Zhao, Y.-X.; Shaw, A.; Zeng, X.; Benson, E.; Nystrom, A. M.; Hogberg, B. DNA Origami Delivery System for Cancer Therapy with Tunable Release Properties. *ACS Nano* **2012**, *6*, 8684–8691.
- Fu, J.; Liu, M.; Liu, Y.; Woodbury, N. W.; Yan, H. Interenzyme Substrate Diffusion for an Enzyme Cascade Organized on Spatially Addressable DNA Nanostructures. *J. Am. Chem. Soc.* **2012**, *134*, 5516–5519.
- Wasielewski, M. R. Self-Assembly Strategies for Integrating Light Harvesting and Charge Separation in Artificial Photosynthetic Systems. *Acc. Chem. Res.* **2009**, *42*, 1910–1921.
- Balzani, V.; Credi, A.; Venturi, M. Photochemical Conversion of Solar Energy. *ChemSusChem* **2008**, *1*, 26–58.
- Lin, C.; Liu, Y.; Yan, H. Designer DNA Nanoarchitectures. *Biochemistry* **2009**, *48*, 1663–1674.
- Seeman, N. C. Nanomaterials Based on DNA. *Annu. Rev. Biochem.* **2010**, *79*, 65.
- Rothenmund, P. W.; Ekani-Nkodo, A.; Papadakis, N.; Kumar, A.; Fygenson, D. K.; Winfree, E. Design and Characterization of Programmable DNA Nanotubes. *J. Am. Chem. Soc.* **2004**, *126*, 16344–16352.
- Yan, H.; Park, S. H.; Finkelstein, G.; Reif, J. H.; LaBean, T. H. DNA-Templated Self-Assembly of Protein Arrays and Highly Conductive Nanowires. *Science* **2003**, *301*, 1882–1884.
- Liu, H.; Chen, Y.; He, Y.; Ribbe, A. E.; Mao, C. Approaching the Limit: Can One DNA Oligonucleotide Assemble into Large Nanostructures? *Angew. Chem., Int. Ed.* **2006**, *45*, 1942–1945.
- Wei, B.; Dai, M.; Yin, P. Complex Shapes Self-Assembled from Single-Stranded DNA Tiles. *Nature* **2012**, *485*, 623–626.
- Kuzuya, A.; Wang, R.; Sha, R.; Seeman, N. C. Six-Helix and Eight-Helix DNA Nanotubes Assembled from Half-Tubes. *Nano Lett.* **2007**, *7*, 1757–1763.

15. Mathieu, F.; Liao, S.; Kopatsch, J.; Wang, T.; Mao, C.; Seeman, N. C. Six-Helix Bundles Designed from DNA. *Nano Lett.* **2005**, *5*, 661–665.
16. Wilner, O. I.; Orbach, R.; Henning, A.; Teller, C.; Yehezkel, O.; Mertig, M.; Harries, D.; Willner, I. Self-Assembly of DNA Nanotubes with Controllable Diameters. *Nat. Commun.* **2011**, *2*, 540.
17. Yin, P.; Hariadi, R. F.; Sahu, S.; Choi, H. M.; Park, S. H.; LaBean, T. H.; Reif, J. H. Programming DNA Tube Circumferences. *Science* **2008**, *321*, 824–826.
18. Douglas, S. M.; Chou, J. J.; Shih, W. M. DNA-Nanotube-Induced Alignment of Membrane Proteins for NMR Structure Determination. *Proc. Natl. Acad. Sci. U. S. A.* **2007**, *104*, 6644–6648.
19. Fu, Y.; Zeng, D.; Chao, J.; Jin, Y.; Zhang, Z.; Liu, H.; Li, D.; Ma, H.; Huang, Q.; Gothelf, K. V. Single-Step Rapid Assembly of DNA Origami Nanostructures for Addressable Nanoscale Bioreactors. *J. Am. Chem. Soc.* **2012**, *135*, 696–702.
20. Mohammed, A. M.; Schulman, R. Directing Self-Assembly of DNA Nanotubes Using Programmable Seeds. *Nano Lett.* **2013**, *13*, 4006–4013.
21. Aldaye, F. A.; Lo, P. K.; Karam, P.; McLaughlin, C. K.; Cosa, G.; Sleiman, H. F. Modular Construction of DNA Nanotubes of Tunable Geometry and Single-or Double-Stranded Character. *Nat. Nanotechnol.* **2009**, *4*, 349–352.
22. Lo, P. K.; Karam, P.; Aldaye, F. A.; McLaughlin, C. K.; Hamblin, G. D.; Cosa, G.; Sleiman, H. F. Loading and Selective Release of Cargo in DNA Nanotubes with Longitudinal Variation. *Nat. Chem.* **2010**, *2*, 319–328.
23. Hamblin, G. D.; Carneiro, K. M.; Fakhouri, J. F.; Bujold, K. E.; Sleiman, H. F. Rolling Circle Amplification-Templated DNA Nanotubes Show Increased Stability and Cell Penetration Ability. *J. Am. Chem. Soc.* **2012**, *134*, 2888–2891.
24. Hamblin, G. D.; Rahbani, J. F.; Sleiman, H. F. Sequential Growth of Long DNA Strands with User-Defined Patterns for Nanostructures and Scaffolds. *Nat. Commun.* **2015**, *6*, 7065.
25. Hariri, A. A.; Hamblin, G. D.; Gidi, Y.; Sleiman, H. F.; Cosa, G. Stepwise Growth of Surface-Grafted DNA Nanotubes Visualized at the Single-Molecule Level. *Nat. Chem.* **2015**, *7*, 295–300.
26. Duzdevich, D.; Redding, S.; Greene, E. C. DNA Dynamics and Single-Molecule Biology. *Chem. Rev.* **2014**, *114*, 3072–3086.
27. Travers, A. The Structural Basis of DNA Flexibility. *Philos. Trans. R. Soc., A* **2004**, *362*, 1423–1438.
28. Liu, J.; Cao, Z.; Lu, Y. Functional Nucleic Acid Sensors. *Chem. Rev.* **2009**, *109*, 1948–1998.
29. Nutiu, R.; Li, Y. Structure-Switching Signaling Aptamers. *J. Am. Chem. Soc.* **2003**, *125*, 4771–4778.
30. Gaudier, M.; Schuwirth, B. S.; Westcott, S. L.; Wigley, D. B. Structural Basis of DNA Replication Origin Recognition by an ORC Protein. *Science* **2007**, *317*, 1213–1216.
31. Jones, S.; van Heyningen, P.; Berman, H. M.; Thornton, J. M. Protein-DNA Interactions: A Structural Analysis. *J. Mol. Biol.* **1999**, *287*, 877–896.
32. Gu, H.; Yang, W.; Seeman, N. C. DNA Scissors Device Used to Measure MutS Binding to DNA Mis-Pairs. *J. Am. Chem. Soc.* **2010**, *132*, 4352–4357.
33. Feng, L.; Park, S. H.; Reif, J. H.; Yan, H. A Two-State DNA Lattice Switched by DNA Nanoactuator. *Angew. Chem.* **2003**, *115*, 4478–4482.
34. Endo, M.; Sugiyama, H. Single-Molecule Imaging of Dynamic Motions of Biomolecules in DNA Origami Nanostructures Using High-Speed Atomic Force Microscopy. *Acc. Chem. Res.* **2014**, *47*, 1645–1653.
35. Johnson-Buck, A.; Nangreave, J.; Jiang, S.; Yan, H.; Walter, N. G. Multifactorial Modulation of Binding and Dissociation Kinetics on Two-Dimensional DNA Nanostructures. *Nano Lett.* **2013**, *13*, 2754–2759.
36. Pinheiro, A. V.; Nangreave, J.; Jiang, S.; Yan, H.; Liu, Y. Steric Crowding and the Kinetics of DNA Hybridization within a DNA Nanostructure System. *ACS Nano* **2012**, *6*, 5521–5530.
37. Ngo, A. T.; Karam, P.; Fuller, E.; Burger, M.; Cosa, G. Liposome Encapsulation of Conjugated Polyelectrolytes: Toward a Liposome Beacon. *J. Am. Chem. Soc.* **2008**, *130*, 457–459.
38. Ulbrich, M. H.; Isacoff, E. Y. Subunit Counting in Membrane-Bound Proteins. *Nat. Methods* **2007**, *4*, 319–321.
39. Casanova, D.; Giaume, D.; Moreau, M.; Martin, J.-L.; Gacoin, T.; Boilot, J.-P.; Alexandrou, A. Counting the Number of Proteins Coupled to Single Nanoparticles. *J. Am. Chem. Soc.* **2007**, *129*, 12592–12593.
40. Hariadi, R. F.; Yurke, B.; Winfree, E. Thermodynamics and Kinetics of DNA Nanotube Polymerization from Single-Filament Measurements. *Chem. Sci.* **2015**, *6*, 2252–2267.
41. Yurke, B.; Turberfield, A. J.; Mills, A. P.; Simmel, F. C.; Neumann, J. L. A DNA-Fuelled Molecular Machine Made of DNA. *Nature* **2000**, *406*, 605–608.
42. Dietz, H.; Douglas, S. M.; Shih, W. M. Folding DNA into Twisted and Curved Nanoscale Shapes. *Science* **2009**, *325*, 725–730.
43. Han, D.; Pal, S.; Nangreave, J.; Deng, Z.; Liu, Y.; Yan, H. DNA Origami with Complex Curvatures in Three-Dimensional Space. *Science* **2011**, *332*, 342–346.
44. Wei, B.; Ong, L. L.; Chen, J.; Jaffe, A. S.; Yin, P. Complex Reconfiguration of DNA Nanostructures. *Angew. Chem.* **2014**, *126*, 7605–7609.